JOURNAL OF PROPULSION AND POWER
Vol. 17, No. 3, May–June 2001

Influence of Compressor Exit Conditions on Combustor Annular Diffusers, Part 1: Diffuser Performance

A. G. Barker* and J. F. Carrotte†
Loughborough University, Loughborough, England, LE11 3TU, United Kingdom

In gas-turbine engines, the velocity of air issuing from the compressor must be reduced to permit effective operation of the downstream combustor. This is partly achieved by locating an annular diffuser behind the compressor outlet guide vanes (OGV) and, in modern systems, the inlet of this diffuser is usually located at the trailing edge of the blade row. The interactions that occur between these components and, in particular, the impact on the measured diffuser performance are studied. A mainly experimental investigation has been undertaken in a fully annular facility that incorporates a single-stage axial-flow compressor and simulated flame tube. In addition, a constant-area passage, or diffusers of area ratio 1.45 or 1.60, can be incorporated immediately downstream of the OGV row. The results indicate that, within experimental error, the diffusers have little effect on the flow within the OGV blade passages. However, the OGV blade row produces a profile that, due mainly to the blade wakes, contains a relatively large amount of kinetic energy. Hence, even within the downstream constant area passage a significant pressure rise is observed as these wakes mix out. Additional pressure forces are introduced with the downstream diffusers present, but analysis of the experimental data indicates these have a limited effect on the wake mixing process, both in terms of stagnation pressure loss and static pressure rise. Hence, the overall static pressure rise measured, between the inlet and exit of each diffuser, is greater than that predicted using design charts obtained using more conventional axisymmetric inlet conditions. This confirms previous work where it was thought that wake mixing can enhance diffuser performance.

Nomenclature

A	=	passage area
AR	=	area ratio
C	=	outlet guide vane (OGV) blade chord
Cp	=	static pressure rise coefficient
h	=	annulus passage height
L	=	diffuser length
m	=	mass flow
N	=	rotor speed
P, p	=	local stagnation, static pressure
R_n	=	nondimensional radius $[(r - r_i)/(r_o - r_i)]$
r	=	radius relative to rig centerline
r_i, r_o	=	inner casing, outer casing radius
s	=	blade pitch
T	=	temperature
U_e	=	mean wake freestream velocity (Fig. 3)
U_f	=	interpolated wake freestream velocity (Fig. 3)
U_m	=	overall mean velocity
u	=	local axial velocity
u_c	=	wake centerline velocity
α	=	kinetic energy flux coefficient based on the overall profile
α_r	=	kinetic energy flux coefficient based on the average radial profile
δ_1	=	wake displacement thickness
δ_3	=	wake kinetic energy displacement thickness
θ	=	wake momentum thickness
λ	=	stagnation pressure loss coefficient

Subscripts

0, 1, 2	=	OGV inlet, diffuser inlet, and diffuser exit traverse planes
mix	=	pressure or velocity after flow is mixed out at constant momentum and area

Superscript

$\bar{}$	=	mass weighted spatial mean value

Received 22 February 2000; revision received 9 July 2000; accepted for publication 9 July 2000.

*Research Assistant, Rolls–Royce University Technology Centre, Department of Aeronautical and Automotive Engineering.

†Rolls–Royce Lecturer in Aerospace Propulsion, Rolls–Royce University Technology Centre, Department of Aeronautical and Automotive Engineering.

Introduction

THE quest for increased power plant performance means that manufacturers continue to focus their attention on the aerodynamic processes taking place within a gas turbine engine. This is achieved both through experimental measurements and the development of numerical codes. However, further performance improvements often mean that consideration must be given to the aerodynamic interactions that occur between components within an engine. This is one of two papers that concentrate on one particular aerodynamic interaction, namely, that which occurs between an axial compressor stage and the annular diffuser that is located immediately downstream. In gas turbine engines the velocity of the air, issuing from the compressor, must be reduced to permit effective operation of the downstream combustor. This is partly achieved by locating an annular diffuser behind the compressor outlet guide vane (OGV) row. Optimization of engine performance means maximizing the velocity reduction within this diffuser, while maintaining a stable flow, before the flow undergoes an abrupt expansion as it enters the combustion system.

Klein[1] reviews numerous diffuser investigations that are relevant to the combustor diffuser application, although most of these investigations have been conducted with nonrepresentative boundary-layer-type inlet conditions. In such investigations the inlet conditions are defined, and surface tappings are used to measure the static pressure rise, within a variety of diffuser geometries. From such experimental work, performance charts have been produced that indicate, for example, the static pressure rise and maximum area ratio, within a given axial length, that can be achieved while avoiding flow separation. This ensure: stable diffuser operation, which is essential for this application. However the different performance charts are obtained with relatively thin[2] or fully developed[3] inlet boundary layers. This reflects the importance of inlet conditions, and Klein[1] outlines the limited data obtained with diffusers located

behind axial compressors. For example, Stevens et al.[4] investigated the performance of a diffuser operating downstream of a multistage axial compressor and also with fully developed inlet conditions. In these investigations overall diffuser performance was assessed, in addition to providing some indication of the mean blade wake profiles and their decay within the diffuser. Further work by Stevens et al.[5] utilized a single-stage compressor whose location, relative to diffuser inlet, could be varied. Hence, the impact on performance of including a parallel passage, between compressor outlet and diffuser inlet, could be assessed. Such a passage was thought necessary to permit the compressor blade wakes to partially mix out prior to entering the diffuser. However, the ever increasing demands for engines of shorter length mean that within modern engines diffusers are often located immediately downstream of the compressor. This, together with diffusers of shorter length, enhances the interaction between the diffuser and compressor-generated flowfields. More recent work by Zierer[6] showed how changing the compressor operating point affected the boundary layers and pressure rise within a diffuser and also noted that, in general, greater pressure rises were achieved with a compressor present. Although no detailed investigations have been conducted, the general conclusion from all of these investigations is that, in addition to the mean flow distribution at the diffuser entrance plane, the enhanced turbulence associated with a compressor-generated flowfield can improve spanwise mixing and thereby reduce boundary-layer growth and the onset of separation.

This investigation concentrates on the effects of wake mixing and secondary flows, due to the presence of an upstream axial flow compressor, on the mean flowfield that develops within a modern combustor annular diffuser geometry. Currently the design of such diffusers is based predominantly on experimental data, obtained with conventional boundary-layer-type inlet conditions, and takes no account of such interactions. It is thought the understanding and capturing of these processes, and their impact on the boundary layers that develop along each casing, is important if a more numerically based method is to be developed for optimizing the design of such diffusers. To assist in defining these processes, results are presented from a mainly experimental investigation in which pneumatic measurements were made, downstream of a single-stage axial flow compressor, as the pressure gradient was varied. This was achieved by using annular diffusers of the same axial length but of area ratios 1.0, that is, parallel passage, 1.45, and 1.60. Furthermore, a flame tube, typical of current gas turbine engine practice, provided a representative blockage to the flow issuing from these diffusers. Note that the distance between the OGV trailing edge and this flame tube was maintained constant in all tests. This particular paper concentrates on the mean flowfield development and its influence on diffuser performance, in terms of the diffuser static pressure rise and the stagnation pressure loss. A subsequent paper (Part 2) outlines how the compressor generated inlet conditions can improve spanwise mixing, within the diffuser, and thereby reduce boundary-layer growth and the onset of separation.

Experimental Facility

A comprehensive description of the overall experimental facility is given by Wray and Carrotte.[7] The working section approximates a large-scale version of a current engine. Air is drawn from atmosphere into a large plenum, above the vertically mounted facility, before passing through the entry flare that contains a honeycomb flow straightener. The pressure rise required to draw air through the facility is provided by the single-stage axial flow compressor located within the working section (Fig. 1). An 80-blade inlet guide vane (IGV) row precedes the rotor, which is operated at a fixed nondimensional condition $[m\sqrt{(T)}/P]$, which corresponds to a flow coefficient of approximately 0.4 and a nondimensional speed $(N/\sqrt{T})$ of 170. For a typical ambient temperature of 291 K, this corresponds to a rotor speed of 2900 rpm, with the rotor providing nominally 45 deg of inlet swirl, at midpassage height, to the compressor OGVs. The mean radius of the IGV, rotor and OGV blade rows is 375 mm,

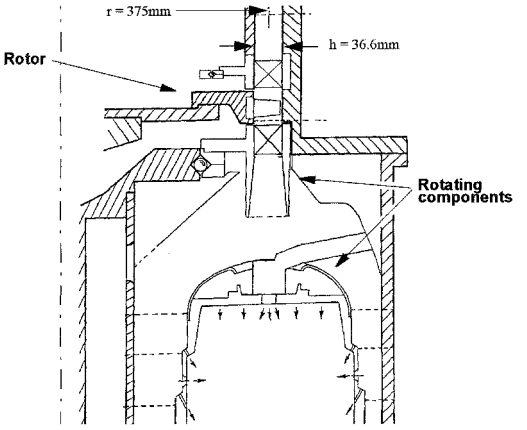

Fig. 1 Test facility.

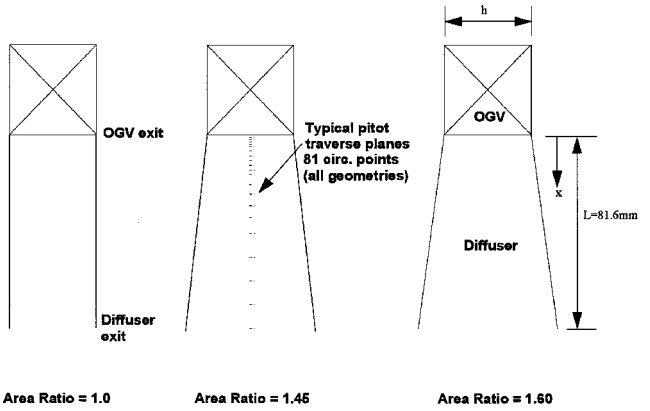

Fig. 2 OGV/diffuser geometries.

with a passage height of 36.6 mm. At a mass flow of 4.6 kg/s, the mean axial velocity through these blade rows is approximately 45 m/s (Mach number ~0.13) with a stage loading of 0.32. Within the facility, various OGV and diffuser geometries can be incorporated, but numerous authors, including Fishenden and Stevens,[8] have also noted the stabilizing effect of the blockage, presented by a downstream flame tube, on the diffuser flow. Hence, at diffuser exit the flow enters a dump cavity, where it divides to pass either into an annular flame tube or to the surrounding feed annuli. Note that porosity of the flame tube head is fully representative, and a series of downstream throttles control the mass flow distribution to the flame tube, feed annuli, and turbine cooling passages. Hence, the blockage downstream of the diffuser is accurately simulated, whereas a further throttle within the exhaust system ensures the axial compressor is maintained on its correct operating point.

For the tests reported here, the OGV row consisted of 160 controlled diffusion blades that were designed to turn the flow through approximately 45 deg. The blades were of chord 39 mm and had a thickness/chord ratio of 6%. At the OGV exit, this same blade row could be attached to diffusers of area ratio 1.00 (parallel passage), 1.45, and 1.60 (Fig. 2), with each diffuser having an axial length of 2.23 inlet passage heights, that is, $2.23h_1$. In addition, the axial length between the OGV exit and the flame tube head was also maintained constant at $3.63h_1$. Note that according to the design criteria obtained with the boundary-layer-type flows described by Howard et al.[3] for a nondimensional length of $2.23h_1$ diffusers of area ratio 1.45 and 1.60 fall within the attached flow regimes, although the latter lies relatively close to the stall line.

Instrumentation

The performance of each diffuser system was defined from measurements at the OGV exit/diffuser inlet $(x/L = 0.00)$ and diffuser

exit ($x/L = 1.00$). Area traverses were performed using miniature five-hole pressure probes of overall diameter 1.5 mm, with hole bore of 0.25 mm, which were used in a nonnulled mode as outlined by Wray and Carrotte.[7] Preliminary measurements confirmed the symmetry of flow, around the annulus, at the diffuser exit after which detailed area traverses were conducted at these two axial locations. At each location, an area corresponding to two OGV blade spaces was traversed with some 820 data points being obtained from 20 radial measurement locations that were repeated at 41 circumferential positions. In addition, five-hole probe traverses were performed on the diffuser centerline, midway between blades, at typically 20 positions between the OGV exit ($x/L = 0.00$) and the exit of each diffuser ($x/L = 1.00$). These measurements were used to provide information on the static pressure rise along the diffuser centerline. Further detailed measurements were obtained with a flattened pitot probe, at midpassage (50%) height, to define the OGV blade wakes. At each of typically 20 axial locations, measurements were obtained at 81 circumferential positions across 2 blade spaces.

Radial movement of the instrumentation, where required, was obtained by attaching the probes to stepper motors located on the outer casing of the facility. In addition, to avoid numerous circumferential access locations, within the diffuser casings, the OGV row and downstream flame tube were mounted on bearings and could, therefore, be indexed to provide the required circumferential movement. Probes of various sizes were inserted, through the rear of the diffuser, with the axial location being varied by attaching the probes to the outer casing at various locations downstream of the diffuser exit plane.

All pressures were logged using Furness pressure transducers, whereas operation of the test rig, positioning of the instrumentation, and digitizing of all pressure transducer signals was controlled by a personal computer.

Data Reduction

Diffuser Performance

The diffuser performance is assessed from area traverses with five-hole pressure probes, at diffuser inlet and exit, that provide information on stagnation and static pressure in addition to velocity magnitude and direction. For the area traverses, this information can be used to derive the overall mean velocity U_m and mass flow through each traverse plane:

$$\dot{m} = \int \rho u \, \mathrm{d}A = \rho U_m A \tag{1}$$

where A is the flow passage area at the plane concerned. Mean values of stagnation pressure $\bar{P}$ were defined by mass weighting the appropriate individual values, that is,

$$\bar{P} = \frac{1}{m} \int_A P \rho u \, \mathrm{d}A \tag{2}$$

For spatially nonuniform incompressible flow, which is in a predominantly axial direction, it also follows that[8]

$$\bar{P} = \bar{p} + \alpha\left(\tfrac{1}{2}\right)\rho U_m^2 \tag{3}$$

where

$$\alpha = \frac{1}{A} \int_A \left(\frac{u}{U_m}\right)^3 \mathrm{d}A, \qquad \bar{p} = \frac{1}{m} \int_A p \rho u \, \mathrm{d}A$$

The kinetic energy flux coefficient α represents the ratio of mass-weighted mean kinetic energy of a nonuniform flow to that of a uniform flow with the same mass flow rate.[8] Note that an alternative definition has also been used, α_r, which is based on a mean radial profile obtained by circumferentially averaging the velocity data, using an area weighting, at a given radial location. A flux coefficient α_r can then be calculated based on this profile, which, therefore, reflects the radial distortion of the flow and its effect on the flow kinetic energy.

Changes in the spatially averaged pressures between planes 1 (OGV exit/diffuser inlet) and 2 (diffuser exit) are expressed in terms of a total pressure loss λ and static pressure rise coefficient Cp, which is nondimensionalized by a reference dynamic head:

$$\lambda = (\overline{P_1} - \overline{P_2})/(\bar{P} - \bar{p})_1, \qquad Cp = (\overline{p_2} - \overline{p_1})/(\bar{P} - \bar{p})_1 \tag{4}$$

Furthermore, as described by Fishenden and Stevens,[8] with the use of Eqs. (1–4) along with the energy equation $\overline{p_1} + \alpha_1(\frac{1}{2})\rho U_{m1}^2 = \overline{p_2} + \alpha_2(\frac{1}{2})\rho U_{m2}^2 + \overline{P_1} - \overline{P_2}$, it follows that

$$Cp = 1 - (\alpha_2/\alpha_1)(1/AR^2) - \lambda \tag{5}$$

which relates the diffuser static pressure rise with that of its stagnation pressure loss, area ratio AR, and flow nonuniformity at inlet and exit.

Wake Profile Definitions

The wake velocity profiles at the midpassage height were obtained from pitot tube measurements, with the static pressure being provided by the five-hole probe. From these data, the following wake displacement, momentum, and kinetic energy thickness values could be calculated:

$$\delta_1 = \int_\delta \left(1 - \frac{u}{U_f}\right) r \, \mathrm{d}\theta, \qquad \theta = \int_\delta \left(\frac{u}{U_f}\right)\left(1 - \frac{u}{U_f}\right) r \, \mathrm{d}\theta$$

$$\delta_3 = \int_\delta \left(\frac{u}{U_f}\right)\left[\left(1 - \frac{u}{U_f}\right)^2\right] r \, \mathrm{d}\theta \tag{6}$$

where U_f is the local wake freestream velocity (Fig. 3). Based on the wake profiles, the mass-weighted stagnation pressure loss,

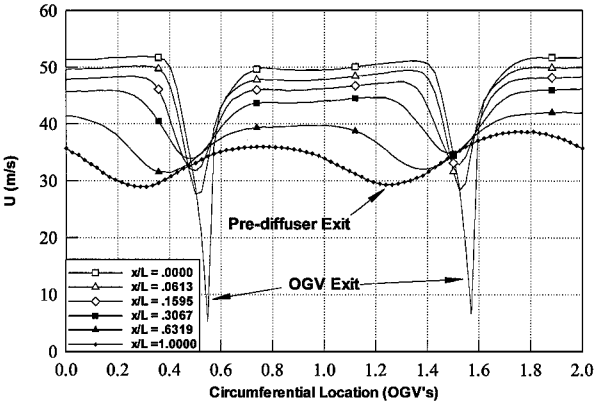

a) Wake axial velocity profiles

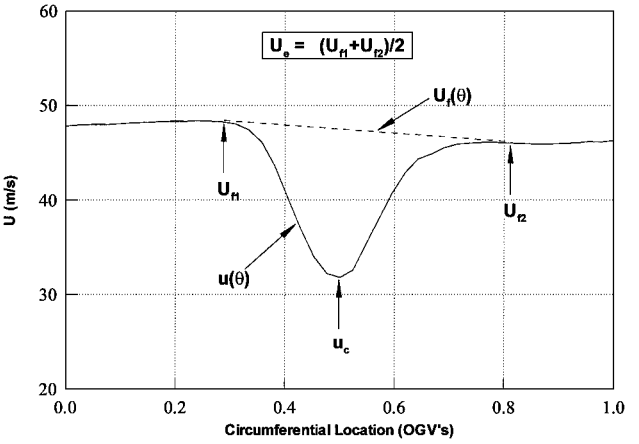

b) Wake velocity definitions

Fig. 3 Circumferential velocity profiles along the diffuser centerline.

associated with the blade wake, ΔP_{mw}, can be calculated at a given axial location from the following definition (see Appendix):

$$\Delta P_{mw} = \frac{0.5U_e^2\delta_3}{(s-\delta_1)} \tag{7}$$

An alternative definition concerns the change in stagnation and static pressure, associated with the wake, if it is allowed to mix out at constant momentum and at the local flow area. These can be derived from the continuity and momentum equations (see Appendix), which, assuming incompressible flow, yield

$$\Delta P_{mix} = \left[(\delta_1/s)^2 + (2\theta/s)\right]\left(0.5\rho U_e^2\right)$$

$$\Delta p_{mix} = \left[(2\delta_1/s)(1-\delta_1/s) - 2\theta/s\right]\left(0.5\rho U_e^2\right) \tag{8}$$

where U_e is the mean wake freestream velocity (Fig. 3). Note that ΔP_{mix} represents the change in stagnation pressure between the local freestream and mixed out values and, therefore, indicates the total loss generated by the blade due to 1) the growth of blade surface boundary layers, and 2) the mixing out of the boundary layers in the blade wake. Alternatively, Δp_{mix} is the change in static pressure between the local measurement plane and the mixed out plane. These wake loss definitions are in broad agreement with the equations quoted by Denton.[9]

Estimate of Experimental Errors

The experimental accuracy of the five-hole probe, in regions of high flowfield gradients, will be influenced by the spatial error associated with the finite distance between the five holes on the probe tip. Attempts were made to reduce this effect by radial and circumferential interpolation of the side pressures onto the central measurement hole, as described by Wray and Carrotte.[7] However, experimental accuracy will also be influenced by the proximity to casing surfaces, recording of the pressure transducer signals via transducers, and an analog-to-digital convertor. Because of these effects, it was found that the mass-weighted stagnation and static pressures at any traverse plane were repeatable to within $\frac{3}{4}$-mm H_2O. Based on these values, it was estimated the stagnation pressure loss λ and static pressure recovery coefficients Cp were accurate to within 0.005 of their true values.

Excellent agreement was obtained for the mass flows calculated at compressor inlet, OGV inlet, and diffuser exit. However, discrepancies in mass flow of up to 2% were recorded at the OGV exit plane and are attributed to the very high gradients at the OGV trailing edge. This leads to errors in velocity and, hence, the kinetic energy flux coefficient α_1. The value of this coefficient was, therefore, obtained using Eq. (5), where all other quantities, including the area ratio, were known. For the pitot probe measurement, there will also be some error in the derived velocity values at this OGV trailing-edge location. This is because immediately behind the blade the static pressure will not equal the value measured in the midpassage region. However, the axial length of this region is relatively small and is thought only to affect the first traverse location $x/L = 0.001$. For quantities derived from the pitot probe measurements, the repeatability was assessed with, for example, the wake displacement thickness δ_1 and momentum thickness θ being repeatable to within 0.1 mm at a given axial location. This can be assessed relative to the wake thickness which, typically, may vary between 5 and 14 mm along the diffuser length.

Results and Discussion

The trailing edge of the OGV blade row is located at inlet to the diffuser, and an indication of the flow distribution, at this location, is provided by the axial velocity contours (Fig. 4). Circumferential variations in the flowfield due to OGV wakes are clearly evident, although the distribution does indicate a relatively well-behaved blade row with no significant regions of flow separation. Note that slight differences between blade passages are due to the influence of wakes from the upstream IGV row, which contains 80 blades (compared with the 160-blade OGV row). Note that within experimental error this distribution was the same for all configurations. Hence, changes at the OGV exit plane, associated with the different diffuser geometries, are small with the diffusers having little impact on the flow within the compressor passages. What must now be established is how this flowfield, thought representative of that generated by a well-behaved compressor stage, influences the performance of a downstream diffuser.

Table 1 Diffuser overall performance data[a]

AR	λ	Cp	α_2	α_{2r}	ΔCp	ΔCp_r
1.00	0.020	0.130	1.037	1.026	0.030	0.020
1.45	0.045	0.520	1.098	1.062	0.040	0.025
1.60	0.060	0.565	1.134	1.089	0.045	0.030

[a]Kinetic energy flux coefficient at diffuser inlet, α_1, is approximately 1.20. All values are nondimensionalized by the kinetic energy at diffuser inlet, that is, $\alpha 0.5\rho U^2$.

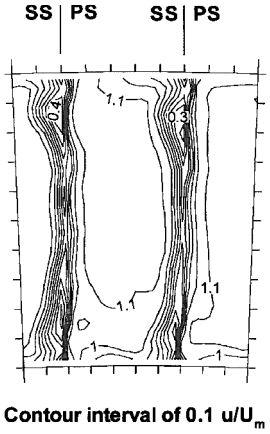

Fig. 4 Axial velocity contours at OGV exit, AR = 1.0.

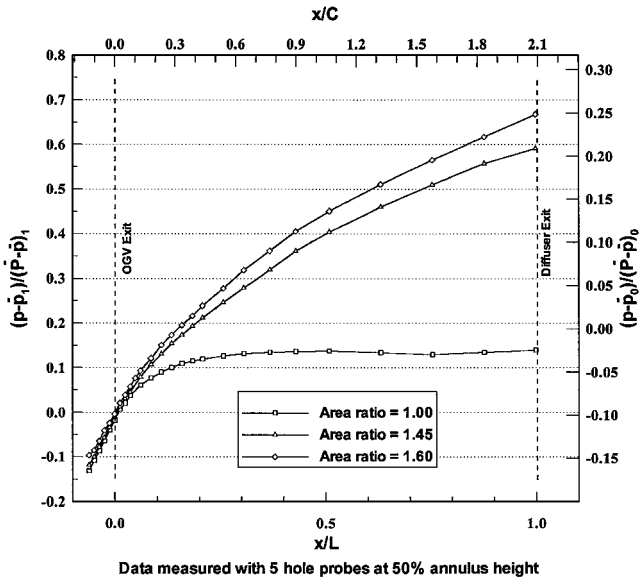

Fig. 5 Static pressure distributions along the diffuser centerlines.

Overall Diffuser Performance

The static pressure distribution measured along the centerline of each diffuser is presented (Fig. 5). Note that axial location is denoted both in terms of diffuser length L and OGV blade chord C, whereas the static pressure rise is in terms of the diffuser inlet dynamic head relative to the static pressure at either OGV inlet or diffuser inlet. In addition, based on the five-hole probe area traverse at the diffuser inlet and exit, the overall static pressure rise Cp and stagnation pressure loss λ coefficients are presented (Table 1).

The distribution of static pressure (Fig. 5) along the constant area passage ($AR = 1.0$) agrees with the overall static pressure rise Cp of 0.130, determined from area traverses at OGV exit and diffuser exit (Table 1). Not surprisingly, as the area ratio is increased to 1.45 and 1.60 the diffuser static pressure rise Cp increases to 0.520 and 0.565, respectively (Table 1). These values, though, are significantly greater than those indicated by the performance charts on which diffusers are often designed. For example, based on these charts zero pressure rise would be expected in a parallel passage ($AR = 1.0$). Furthermore, with the diffusers present and fully developed inlet conditions, the results of Howard et al.[3] indicate static pressure rises of approximately 0.37 ($AR = 1.45$) and 0.38 ($AR = 1.60$), whereas the more uniform conditions of Sovran and Klomp[2] indicate a pressure rise of approximately 0.40 for both diffuser geometries. Note that in both cases the inlet flow was axisymmetric with the nonuniformity being in the radial profile only, and furthermore, in these investigations the pressure coefficient was nondimensionalized by the diffuser inlet dynamic head ($\frac{1}{2}\rho U_m^2$). Hence, differences in the static pressure rise will be even greater when the kinetic energy flux coefficient α is included. In these other investigations, the static pressure rise was obtained from tappings within each diffuser, and the inlet profile was also measured. However, the exit profile was not measured, and so insufficient information is available for the stagnation pressure loss within each diffuser to be predicted. For this investigation though, the stagnation pressure loss λ measured within the constant area passage was 0.020, and this increased to 0.045 ($AR = 1.45$) and 0.060 ($AR = 1.60$) with increasing diffuser area ratio.

The static pressure rise within each diffuser is determined by the area ratio, the stagnation pressure loss, and the kinetic energy of the flow entering and leaving the diffuser [Eq. (5)]. At diffuser inlet, the kinetic energy coefficient value α_1 is approximately 1.20 and indicates a relatively large amount of kinetic energy is present at the trailing edge of even a well-behaved blade row. This flow then enters the diffuser system, and its subsequent development will have a significant effect on the observed static pressure rise and stagnation pressure loss. For example, the axial velocity contours at the diffuser exit are presented for the area ratio 1.0 (parallel passage) and 1.60 diffusers (Fig. 6). Note that for both geometries the flow has remained attached to the casings at all circumferential locations, and comparison with the diffuser inlet contours (Fig. 4) shows that some mixing out of each OGV wake has occurred. However, both the amount of mixing and the growth of low-energy fluid adjacent to each casing varies between configurations. Such distributions also indicate the complexity of the flowfield and highlight differences relative to more conventional diffuser investigations with axisymmetric inlet conditions. Nonetheless, an attempt can be made to assess how these various flow features, as found within a turbomachine environment, influence the diffuser static pressure rise and stagnation pressure loss.

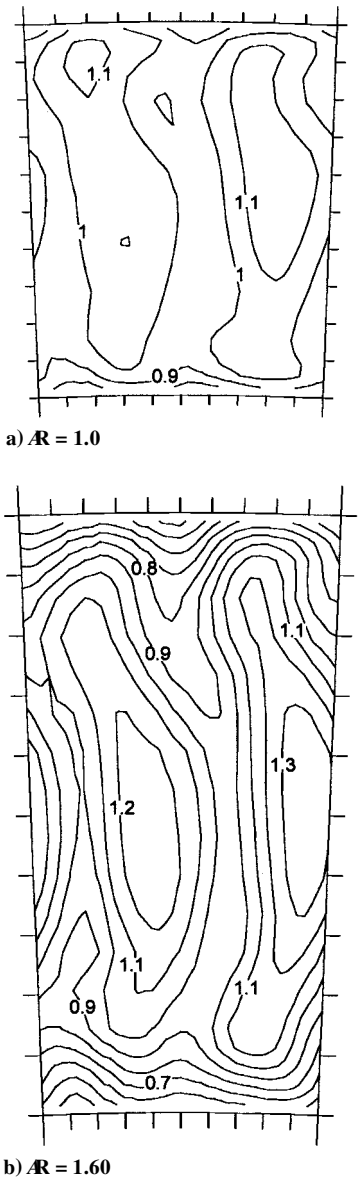

Fig. 6 Axial velocity contours (u/U_m) at diffuser exit.

Diffuser Radial Profiles

The acceleration or deceleration of a fluid particle passing through each diffuser is mainly a function of the shear forces, acting on the particle, along with the pressure forces associated with the applied pressure gradient. In addition, the momentum equation indicates that the sensitivity of a particle to this pressure gradient is much greater if its velocity is relatively low. With more conventional axisymmetric inlet conditions it is, therefore, the radial profile and, in particular, the slower moving fluid within the casing boundary layers that is of most concern. Hence, the resulting growth of the boundary layer with increasing area ratio produces a more distorted radial profile, which, relative to a uniform profile, contains a greater amount of kinetic energy. This affects the static pressure rise, as reflected by the diffuser performance charts, whereas the onset of transitory stall and unstable flow regimes is associated with the separation of these boundary layers from the casing surface.

The axial velocity contours at OGV exit (Fig. 4) and diffuser exit (Fig. 6) indicate the more complex flowfield that is introduced by the upstream compressor. Furthermore, although mean radial profiles can be obtained by circumferentially averaging the data at each radial location (Fig. 7), the profiles do not indicate clearly defined boundary layers. For example, variations in the radial profile occur due to high loss regions associated with the remnants of endwall losses within the OGV passage. With an upstream compressor present, investigations by authors such as Stevens et al.[5] and Klein[1] have indicated, for pressure gradients typical of the gas turbine application being considered, that radial distortions are amplified if distortion of the radial profile entering the diffuser is relatively weak. Alternatively, if the initial distortion is large, then the radial distortions will decay. Presumably this reduction is due to the shear stresses associated with highly distorted radial velocity profiles. As outlined by Klein,[1] strong radial distortions may, for example, be generated by OGV rows with radial blade clearances. However, the results of the current investigation indicate that blade geometries typical of current modern systems generate weak radial distortions, and this is reflected by the observed profile development within the downstream diffusers (Fig. 7). Hence, for the constant area passage ($AR = 1.0$), the profiles are virtually identical along the passage, but with increasing area ratio, more distorted profiles develop and reflect the migration of fluid toward the passage center. Thus, the radial profile development is being dominated by the imposed pressure forces rather than the shear forces.

Development of the radial profiles within each geometry are summarized by the radial kinetic energy flux coefficient α_r, which can

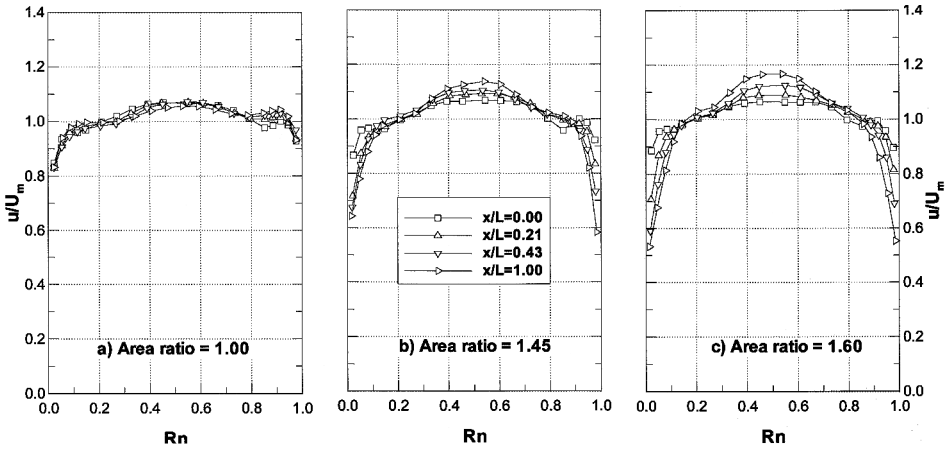

Fig. 7 Circumferentially averaged diffuser velocity profiles.

be compared with the overall flux coefficient values α entering and leaving each diffuser. As already indicated [Eq. (5)], these values affect the overall pressure rise Cp. For example, note that in all cases the diffuser exit flux coefficient values α_2 of 1.037 ($AR = 1.00$), 1.098 ($AR = 1.45$), and 1.134 ($AR = 1.60$) are less than the diffuser entry value of approximately 1.20. Based on Eq. (5), this accounts for the relatively high static pressure rise values Cp obtained for these geometries relative to that indicated by the diffuser performance charts. However, based on the radial profiles, α_r, the inlet value of 1.028 can be compared with the exit values of 1.026 ($AR = 1.00$), 1.062 ($AR = 1.45$), and 1.089 ($AR = 1.60$). Thus, reduction in the overall distortion of the flowfield within each diffuser means the increasing radial distortion is being offset by a reduction in the circumferential distortions. Therefore, it follows that mixing out of the blade wakes is responsible for the high static pressure rise relative to that obtained from tests with axisymmetric inlet conditions. With this in mind, attempts can be made to assess the significance of OGV mixing on diffuser performance and, furthermore, how wake mixing is affected by the presence of a downstream diffuser.

OGV Wake Mixing (Midpassage Height)

The influence of OGV wakes on the diffuser static pressure rise and stagnation pressure loss has been assessed by analyzing the mixing out of blade wakes along the centerline of each diffuser. This has been undertaken for the datum case when the wakes mix out in a parallel passage, and the differences were then noted when the diffusing passages were introduced. It is assumed that these changes in wake behavior along the centerline are a reflection of those occurring across most of the blade height. Hence, what can also be implied is how the remainder of the flow, that is, low-energy boundary-layer-type fluid adjacent to each casing, is contributing to the overall performance for the different passage geometries.

Wake Parameters

At a given axial location, the blade wakes were defined from measurements at 81 circumferential positions that were equally spaced across two OGV blade passages. These measurements were repeated at up to 20 axial locations within each diffuser. Development of the blade wakes within the 1.45 area ratio diffuser is indicated by the measured profiles, although, for clarity, only a limited number are presented (Fig. 3a). Note that at a given axial location the freestream velocity variations are due to the remnants of effects associated with the upstream IGV row. However, these variations impact on the calculation of parameters such as the wake displacement thickness. A linear variation of the freestream velocity U_f has, therefore, been assumed, across the wake, when calculating such parameters from which a mean freestream velocity U_e can also be derived (Fig. 3b).

A general indication of the wake behavior is provided by the integral-based quantities such as the variation of form parameter H and displacement thickness δ_1 along each diffuser centerline

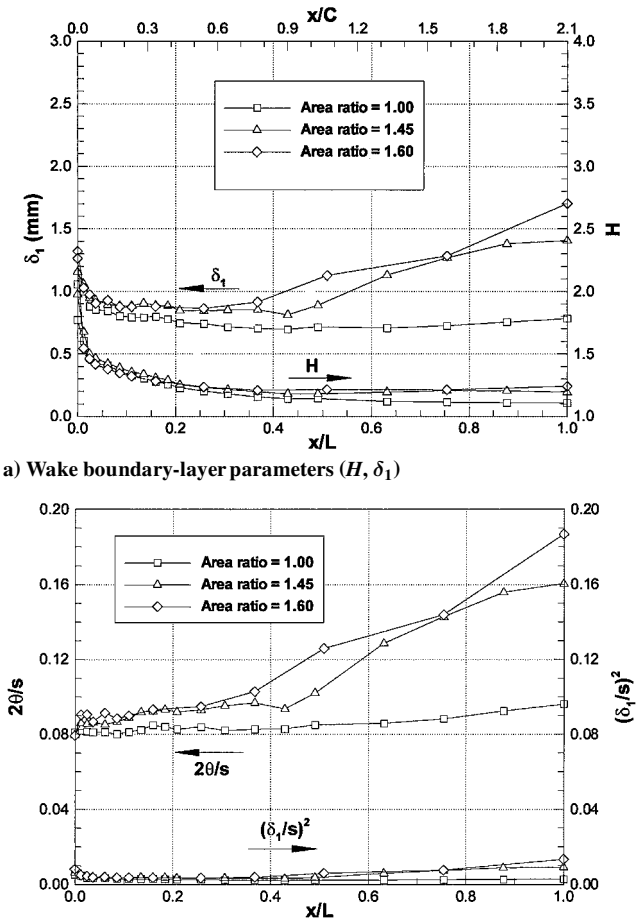

a) Wake boundary-layer parameters (H, δ_1)

b) Mixing loss components [$2\theta/s$, $(\delta_1/s)^2$]

Fig. 8 Wake parameters along each diffuser, 50% passage height.

(Fig. 8a). It is from these various parameters that the most significant factors influencing the wake development can be determined. For example, the initial reduction in form parameter H, immediately downstream of each OGV blade, indicates the rapid mixing that occurs due to the shear stresses associated with the high-velocity gradients in the wakes. This is despite the pressure gradients that are present immediately downstream of the blade row and that vary between geometries (Fig. 5). The relatively large magnitude of the shear forces, therefore, means that, in every geometry, the form parameter H falls to a value of approximately 1.2 within half a chord of the blade trailing edge (Fig. 8a). However, as the velocity gradients, and hence shear stresses, reduce, the pressure forces become of greater significance, and so differences are more apparent toward

the rear of each diffuser. This is most clearly illustrated by the wake displacement thickness. In all of the geometries, the displacement thickness due to the shear forces reduces from approximately 1.2 to 0.8 mm within half a chord of the blade trailing edge; however, downstream of this location, the displacement thickness increases as the area ratio and, hence, pressure forces increase. Thus at the diffuser exit, displacement thickness values of 0.8 and 1.7 mm are obtained for the 1.00 and 1.60 area ratio passages.

These measurements have been made on geometries in which the length and aspect ratio of the OGVs and diffusers are thought to be reasonably representative of modern engines. However, it should be remembered that these observations are a function of the OGV chord relative to the diffuser length. For example, a blade of higher aspect ratio and, hence, shorter chord would reduce and increase the respective lengths over which the shear and pressure forces dominate within the diffuser.

Influence on Stagnation Pressure Loss

The mixing loss value ΔP_{mix} defined in Eq. (8) represents the stagnation pressure loss generated by the OGV blade, that is, it is the mixed out loss and, therefore, represents the difference between the local freestream stagnation pressure and the mixed out stagnation pressure. By definition, for the constant area passage ($AR = 1.0$), this mixing loss value ΔP_{mix} should be constant, but the calculated values increase from, for example, 0.048 ($x/L = 0.20$) to 0.052 ($x/L = 1.0$). Note that because the mixing loss values include the OGV loss these values have been nondimensionalized by the dynamic head at the OGV inlet $\Delta P_{\text{mix}}/(\bar{P} - \bar{p})_o$. It is thought that the increasing mixing loss along each passage is due to a radial redistribution of flow associated with the secondary flows, generated within the upstream blade row, and is the subject of a future paper. An alternative method has, therefore, been used to assess the approximate impact of the diffusing pressure gradient on the mixing loss. When Eq. (8) is differentiated and the momentum and continuity equations are used, then the change in mixing loss is defined as

$$\frac{\mathrm{d}}{\mathrm{d}x}\Delta P_{\text{mix}} = \frac{1}{U_{\text{mix}}}\frac{\mathrm{d}U_{\text{mix}}}{\mathrm{d}x}\left[2\left(\frac{\delta_1}{s}\right)^2 + \frac{2\theta}{s} - \frac{2\theta}{s}H\right]\left(0.5\rho U_e^2\right) \quad (9)$$

where U_{mix} is the mixed out (or mean) velocity and x is the distance along the wake. Furthermore, as defined in Eq. (8) and described by Denton,[9] the mixing loss is composed of 1) the mixed out loss of the blade surface boundary layers ($2\theta/s$) and 2) that associated with the blockage of these boundary layers (δ_1/s). This latter effect is due to the pressure rise and, hence, loss increment that occurs as the blade surface boundary layers mix out, that is, as indicated by the measured pressure distribution within the parallel passage. The values of these terms within each geometry is presented (Fig. 8b) and indicate that the loss is dominated by the first term. With this in mind, the increase in stagnation pressure loss ΔP_{mix} that would be obtained from a mixing calculation at the local flow area [Eq. (9)] can be simplified to

$$\frac{\mathrm{d}}{\mathrm{d}x}\Delta P_{\text{mix}} = \frac{1}{U_{\text{mix}}}\frac{\mathrm{d}U_{\text{mix}}}{\mathrm{d}x}[\Delta P_{\text{mix}}(1 - H)] \quad (10)$$

Equation (10) agrees with that quoted by Denton,[9] and when the measured values of form parameter H and local velocity U_{mix} are used, this has been used to calculate the additional mixing loss due to the applied pressure gradients within each diffuser (Fig. 9). Thus, at the midpassage height, the mixed out OGV loss is 0.053 ($AR = 1.0$) but this increases by 0.005 (~9%) and 0.006 (~11%) for the 1.45 and 1.60 area ratio diffusers. These values are nondimensionalized by the OGV inlet dynamic head and so, when based on the diffuser inlet conditions, a loss increase of order 0.01 is indicated with the diffusers present. Note that this represents a maximum because 1) it is assumed all of the mixing loss occurs within the diffusers and 2) it assumes this loss is realized across the whole of the passage height. This loss increment, of order 0.01, can be compared (Table 1) with the measured mass-weighted loss values, which increase from 0.019 ($AR = 1.00$) to 0.043 ($AR = 1.45$) and 0.058 ($AR = 1.60$). Hence, the largest contribution to the loss increase within the diffusing passages is associated with the boundary-layer growth along each casing rather than the additional loss due to wake mixing within a positive pressure gradient.

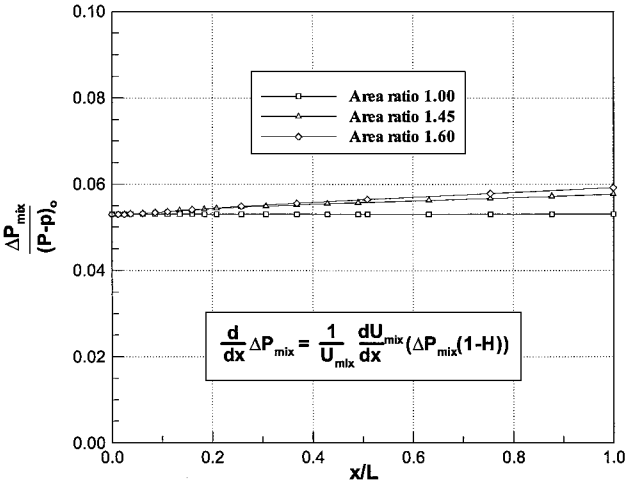

Fig. 9 Mixing loss increase along each diffuser (ΔP_{mix}).

Influence on Static Pressure

It has already been noted that the kinetic energy flux coefficient α value of 1.20 at the inlet of each diffuser is greater than the values of 1.037 ($AR = 1.0$), 1.098 ($AR = 1.45$), and 1.134 ($AR = 1.60$) at the exit of these passages. Hence, despite a more distorted radial profile (Table 1), mixing out of the blade wakes helps reduce the kinetic energy associated with the overall flow profile and thereby produces a static pressure rise. For example, in the parallel passage ($AR = 1.0$) case the initial rapid mixing, within half a chord of the blade trailing edge, leads to a reduction in wake displacement thickness (Fig. 8a). Hence, the effective area of the passage increases, which accounts for the observed rise in static pressure (Fig. 5). Although this pressure rise occurs within the downstream passage, it is a remnant of the inlet flow conditions that are being generated by the upstream blade row, that is, some 10% of the static pressure increase associated with the OGV row is occurring within the downstream passage. However, what must be considered is how this wake mixing process and, hence, the static pressure rise are affected when this process occurs within a diffusing passage typical of those used within a gas turbine engine.

Because of the magnitude of the shear forces, an initial pressure increase occurs within the diffuser geometries, but in these cases it is superimposed on the additional static pressure rise due to the changing geometric passage area (Fig. 5). Within these cases, though, the applied pressure forces associated with the increasing passage area eventually cause the wake displacement thickness to increase (Fig. 8a). This increase can be assessed relative to the blade pitch (14.72 mm) so that, for the centerline flow, the wake blockage at the diffuser exit increases from 5.5% ($AR = 1.0$) to 11.5% ($AR = 1.60$). This, of course, will reduce the static pressure rise within the diffuser; however, note that the increasing displacement thickness is occurring as the local velocity is reducing. Hence, the effect of this blockage on the overall diffuser pressure rise is limited. This is illustrated (Fig. 10) by the mixed out static pressure values Δp_{mix} defined by Eq. (8). At a given axial location, this represents the change in static pressure between the measured value at that location and the value that would be obtained if the flow were allowed to mix out at that local flow area. Hence, a value, Δp_{mix}, of zero indicates the blade wakes are fully mixed out, and the maximum static pressure rise associated with this wake mixing has been achieved. Hence, most of the pressure rise associated with mixing out of the blade wakes is obtained with only small differences being apparent toward the diffuser exit. This agrees with the ΔCp and ΔCp_r values already presented (Table 1) that quantify the additional pressure

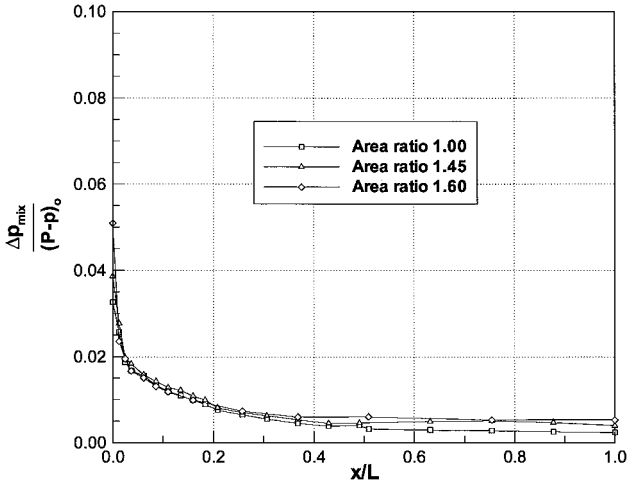

Fig. 10 Mixed out static pressure distribution along each diffuser (Δp_{mix}).

rise that would be achieved if the overall diffuser exit profile, ΔCp, or the radial distortions only, ΔCp_r, were to mix out. As a broad estimate, the static pressure rise of 0.130 achieved within a constant area passage will be offset by an increase in stagnation pressure loss ($\sim$0.01) and effects due to more distorted wakes ($\sim$0.01) for the 1.60 area ratio diffuser. Nevertheless, this still indicates a static pressure rise Cp contribution in excess of 0.11, within the 1.60 area ratio diffuser, that is associated with the mixing out of the circumferential blade wake distortions.

In summary, a relatively large amount of kinetic energy is presented to the downstream passages because of the circumferential distortions associated with the blade wakes. However, the high shear forces produce a rapid mixing out of the blade wakes in each geometry. In terms of the static pressure rise, this effect is of greater magnitude compared with the slight increase in stagnation pressure loss and the effects on wake mixing, due to the imposed pressure forces, within the diffusing passages. This is also thought to account for 1) the relatively high static pressure rise measured by many authors in gas turbine applications relative to that of published performance charts and 2) why in modern systems the diffuser is located immediately downstream of the blade row as opposed to a parallel mixing passage that, in earlier gas turbine systems, was located between the OGV row and diffuser. Note also this additional pressure rise is not associated with a superior diffuser design, but merely the remnants of the static pressure rise and flowfield produced by the upstream OGV row.

Conclusions

Measurements have been made behind a single-stage compressor in which, immediately downstream of the OGV row, the pressure gradient has been varied by using either a parallel passage or diffusers of area ratios 1.45 and 1.60. The OGV blading and diffusers simulate the flows generated within a modern combustor diffuser system, and the following conclusions have been drawn.

1) The mass-weighted stagnation pressure loss λ, between the OGV exit and diffuser exit, increases from 0.020 (parallel passage) to 0.045 and 0.060 for the 1.45 and 1.60 area ratio diffusers. The increase in loss associated with wake mixing, due to the additional pressure gradients associated with the diffusing passages, is of order 0.01, and so most of the loss increase is associated with the low-energy flow adjacent to each casing.

2) At the OGV blade row trailing edge, the flow profile contains a relatively large amount of kinetic energy due to the blade wakes. In a parallel passage, some 10% of the pressure rise associated with the OGV blade row, therefore, occurs in the downstream passage as the blade wakes mix out.

3) Despite the additional pressure forces introduced by the presence of diffusing passages, the high shear forces, associated with the blade wakes, ensure that circumferential flow distortions decrease.

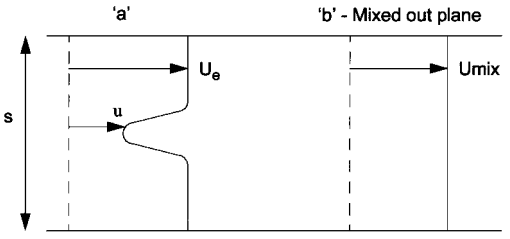

Fig. A1 Wake mixing definitions.

However, the pressure forces do result in the development of more distorted radial profiles along each diffuser.

4) The static pressure rise measured between OGV exit and diffuser exit increases from 0.130 (parallel passage) to 0.520 and 0.565 for the 1.45 and 1.60 area ratio diffusers. The small change in the wake profiles and mixing losses, between the different geometries, indicates that virtually all of the pressure rise associated with the wake mixing also occurs with the diffusers present.

In general, the results indicate that the initial shear forces are large relative to the pressure gradients associated with the diffusing passages. Hence, the performance penalty associated with the mixing of wakes in a diffuser, whose inlet is located at the OGV trailing edge, is small. Furthermore, it also seems relevant to assess the overall performance of the OGV/diffuser system, rather than attempting to assess the performance of these components in isolation.

Appendix: Wake Definitions

Consider a wake, at plane a, within a constant area duct (Fig. A1) for which the mass flow will be $\rho U_e(s-\delta_1)$. The mass-weighted stagnation pressure loss ΔP_{mw} associated with the reduction in pressure within the wake is given by

$$\Delta P_{\mathrm{mw}}\rho U_e(s-\delta_1) = \frac{1}{2}\int \left(U_e^2 - u^2\right)\rho u \, \mathrm{d}y$$

from which

$$\Delta P_{\mathrm{mw}} = \frac{0.5U_e^2\delta_3}{(s-\delta_1)} \tag{A1}$$

Now if the wake at plane a mixes out, within the duct, to a uniform profile at plane b (Fig. A1) then the following equations apply.

Continuity:

$$m = \rho U_e(s-\delta_1) = \rho U_{\mathrm{mix}} s \tag{A2}$$

Momentum:

$$p_a s + \rho U_e(s-\delta_1) - \rho U_e^2 = p_b s + \rho s U_{\mathrm{mix}}^2 \tag{A3}$$

Note also that the freestream stagnation pressure at plane a is given by $(p_a + 0.5\rho U_e^2)$ and that the stagnation pressure at plane b is $(p_b + 0.5\rho U_{\mathrm{mix}}^2)$. These equations can be manipulated to provide an expression for the change in stagnation pressure between the freestream value, at plane a and the mixed out value, that is,

$$\Delta P_{\mathrm{mix}} = \left[(\delta_1/s)^2 + (2\theta/s)\right]\left(0.5\rho U_e^2\right) \tag{A4}$$

Similarly, the change in static pressure between the freestream value at plane a and the mixed out value is given by

$$\Delta p_{\mathrm{mix}} = [(2\delta_1/s)(1-\delta_1/s) - 2\theta/s]\left(0.5\rho U_e^2\right) \tag{A5}$$

Acknowledgments

The authors would like to acknowledge D. Glover, L. Monk, and W. Nivin for their assistance in the manufacture of the test rig and A. P. Wray for his help in the mechanical design of this facility. In addition, the helpful comments of S. J. Stevens and J. Denton are also greatly appreciated.

References

[1]Klein, A., "Characteristics of Combustor Diffusers," *Progress in Aerospace Sciences*, Vol. 31, No. 3, 1995, pp. 171–271.

[2]Sovran, G., and Klomp, E., "Experimentally Determined Optimum Geometries for Rectilinear Diffusers with Rectangular, Conical or Annular Cross-Section," *Fluid Mechanics of Internal Flow*, Elsevier, New York, 1967, pp. 270–312.

[3]Howard, J. H. G., Henseler, H. J., and Thornton-Trump, A. B., "Performance and Flow Regimes for Annular Diffusers," American Society of Mechanical Engineers, ASME Paper 67-WA/FE-21 (A68-11861), June 1967.

[4]Stevens, S. J., Nayak, U. S. L., Preston, J. F., Robinson, P. J., and Scrivener, C. T. J., "Influence of Compressor Exit Conditions on Diffuser Performance," *Journal of Aircraft*, Vol. 15, No. 8, 1978, pp. 482–488.

[5]Stevens, S. J., Harasgama, S. P., and Wray, A. P., "Influence of Blade Wakes on the Performance of Combustor Shortened Prediffusers," *Journal of Aircraft*, Vol. 21, No. 9, 1984, pp. 641–648.

[6]Zierer, T., "Experimental Investigation of the Flow in Diffusers Behind an Axial Flow Compressor," American Society of Mechanical Engineers, ASME Paper 93-GT-347, May 1993.

[7]Wray, A. P., and Carrotte, J. F., "The Development of a Large Annular Facility for Testing Gas Turbine Combustor Diffuser Systems," AIAA Paper 93-2546, July 1993.

[8]Fishenden, C. R., and Stevens, S. J., "Performance of Annular Combustor-Dump Diffusers," *Journal of Aircraft*, Vol. 14, No. 1, 1977, pp. 60–67.

[9]Denton, J. D., "Loss Mechanisms in Turbomachines," *Journal of Turbomachinery*, Vol. 115, No. 4, 1993, pp. 621–656.